
Article:
Henkel, S, Kasten, S, Poulton, SW et al. (1 more author) (2016) Determination of the stable iron isotopic composition of sequentially leached iron phases in marine sediments. Chemical Geology, 421. 93 - 102. ISSN 0009-2541

https://doi.org/10.1016/j.chemgeo.2015.12.003

Determination of the stable iron isotopic composition of sequentially leached iron phases in marine sediments

Susann Henkel[1,2], Sabine Kasten[2], Simon W. Poulton[3], and Michael Staubwasser[1]

[1] University of Cologne, Zülpicher Str. 49a, 50674 Cologne, Germany

[2] Alfred Wegener Institute, Helmholtz Centre for Polar and Marine Research, Am Handelshafen 12, 27570 Bremerhaven, Germany

[3] School of Earth and Environment, The University of Leeds, Leeds, LS2 9JT, United Kingdom

Corresponding author: Susann Henkel (susann.henkel@awi.de)

Abstract

Reactive iron (oxyhydr)oxide minerals preferentially undergo early diagenetic redox cycling which can result in the production of dissolved Fe(II), adsorption of Fe(II) onto particle surfaces, and the formation of authigenic Fe minerals. The partitioning of iron in sediments has traditionally been studied by applying sequential extractions that target operationally-defined iron phases. Here, we complement an existing sequential leaching method by developing a sample processing protocol for δ^{56}Fe analysis, which we subsequently use to study Fe phase-specific fractionation related to dissimilatory iron reduction in a modern marine sediment. Carbonate-Fe was extracted by acetate, easily reducible oxides (e.g. ferrihydrite and lepidocrocite) by hydroxylamine-HCl, reducible oxides (e.g. goethite and hematite) by dithionite-citrate, and magnetite by ammonium oxalate. Subsequently, the samples were repeatedly oxidized, heated and purified via Fe precipitation and column

chromatography. The method was applied to surface sediments collected from the North Sea, south of the Island of Helgoland. The acetate-soluble fraction (targeting siderite and ankerite) showed a pronounced downcore δ^{56}Fe trend. This iron pool was most depleted in ^{56}Fe close to the sediment-water interface, similar to trends observed for pore-water Fe(II). We interpret this pool as surface-reduced Fe(II), rather than siderite or ankerite, that was open to electron and atom exchange with the oxide surface. Common extractions using 0.5 M HCl or Na-dithionite alone may not resolve such trends, as they dissolve iron from isotopically distinct pools leading to a mixed signal. Na-dithionite leaching alone, for example, targets the sum of reducible Fe oxides that potentially differ in their isotopic fingerprint. Hence, the development of a sequential extraction Fe isotope protocol provides a new opportunity for detailed study of the behavior of iron in a wide-range of environmental settings.

Keywords

Iron, sediment, sequential extraction, stable Fe isotopes, early diagenesis

1 Introduction

The many aspects of the biogeochemical cycle of Fe, such as sources and sinks, changes in redox state, and phase transformations have been intensely studied in continental and marine environments. Iron fluxes and the bioavailability of respective Fe mineral phases, however, are still poorly constrained (Raiswell and Canfield 2012), mainly due to methodological challenges in tracing the complex reaction pathways in which Fe participates. As early as the 1960s and 1970s, the need for separation of (highly) reactive Fe minerals from unreactive phases led to the development of sequential chemical extraction

methods (e.g. Mehra and Jackson 1960, Schwertmann 1964, McKeague and Day 1966, Tessier et al. 1979). Since then these schemes have been modified to enhance their selectivity (e.g. Lord III 1980, Phillips and Lovley 1987, Cornwell and Morse 1987, Ferdelman 1988, Canfield 1988, Kostka and Luther 1994, Haese et al. 1997, Hyacinthe and Van Capellen 2004, Poulton and Canfield 2005, Raiswell et al. 2010). Although operationally-defined and not entirely mineral-specific, these methods are now routinely applied in soil and sediment biogeochemical studies. In soil science, Fe solid phase speciation and distribution patterns are used to classify soils and to reconstruct pedogenesis (e.g. Wiederhold et al. 2007a). Soil Fe mineralogy has been shown to control the mobility of pollutants and other nutrients (Stucki et al. 1988).

Fe extractions in modern marine sediments have often been performed to identify the pool of Fe that is potentially reducible during early diagenesis, either through dissimilatory iron reduction (DIR) (e.g. Slomp et al. 1997, Jensen et al. 2003), or by direct abiotic reduction with dissolved sulphide (e.g. Canfield et al. 1992, Poulton et al. 2004). These extraction procedures have also widely been used to study and quantify the post-depositional alteration of the primary Fe mineral assemblage – including the overprint of rock magnetic characteristics of sediments (e.g. Kasten et al. 1998, Riedinger et al. 2005, März et al. 2008). Furthermore, reactive Fe oxide minerals buried and preserved in subsurface marine sediments have recently been suggested to be an important substrate in the anaerobic oxidation of methane (e.g. Beal et al. 2009, Segarra et al. 2013, Riedinger et al. 2014, Sivan et al. 2011, 2014, Egger et al. 2015). Similarly, for ancient sediments, the analysis of sequentially leached solid phase iron species in black shales and banded iron formations, has revealed important insight into the redox-state of the past ocean (e.g. Poulton and Canfield 2011).

A growing number of studies on Fe sources to the ocean, and reaction pathways in the modern or ancient marine environment, have focused on, or have been complemented by, stable Fe isotope analysis (e.g. Anbar and Rouxel 2007, Johnson et al. 2008, Conway and John 2014). In particular, biologically-driven redox cycling initiated by DIR may lead to a specific Fe isotope compositional fingerprint, which distinguishes such Fe from other sources, such as hydrothermal fluids, river discharge, and dust deposition (Beard et al. 2003a, Severmann et al. 2010, Homoky et al. 2009, 2013). However, experimental studies – biotic and abiotic – demonstrate the complexity of Fe isotope fractionation during specific reaction pathways and between the Fe mineral phases involved. For example, isotope fractionation occurs between dissolved Fe, surface-bound Fe, and the bulk of the Fe-oxide mineral during both DIR (Crosby et al. 2007) and abiotic equilibrium exchange (Wu et al. 2011). During pyrite formation, Fe isotopes fractionate between dissolved Fe, mackinawite, and pyrite (Guilbaud et al. 2013). The use of Fe isotopes as a fingerprint for a specific source or reaction pathway may therefore require analytical discrimination between different Fe phases.

Sequential leaching techniques may provide the means to address the above isotopic complexity. Initial studies have shown, for example, that the isotopic fingerprint of DIR in marine sediments is detectable only in the reactive Fe oxides (Severmann et al. 2006, Staubwasser et al. 2006). Similarly, the first Fe isotope data obtained from partial selective leaching of soils has provided valuable insight into the weathering of Fe minerals and their utilization as nutrient sources during plant growth (Wiederhold 2007b, Guelke et al. 2010). In an attempt to address Fe fluxes to the ocean, Scholz et al. (2014) used Fe concentration data from sequential leaching extracts, in combination with Fe isotope data from HCl leaching, to identify diagenetic Fe recycling into the water column on the eastern Pacific

margin. The logic next step is to apply Fe isotope analyses directly to a full sequential leaching protocol. However, there are a number of analytical issues that must be solved prior to application, such as potential isotope fractionation during the Fe separation chemistry required for isotope analysis, and matrix-induced mass bias from residual leaching chemicals during mass spectrometry.

Here, we have developed a protocol to measure Fe isotopes in different operationally-defined Fe pools targeted by a commonly used extraction procedure for modern and ancient sediments (Poulton and Canfield 2005; henceforth referred to as the PC-Method). The method was developed mainly to study the redox evolution of depositional environments recorded in sedimentary archives, but is more broadly applicable to studies of Fe biogeochemistry in modern and ancient settings. The PC-Method targets a variety of ´highly reactive´ Fe phases, including carbonate Fe (e.g. siderite) with acetic acid, easily reducible Fe hydroxides and oxyhydroxides (ferrihydrite, lepidocrocite) with hydroxylamine-HCl, reducible (oxyhydr)oxides (goethite, hematite, akaganéite) with a solution of Na-dithionite and Na-citrate, and magnetite with oxalic acid. Some of these leaching steps have been applied in earlier Fe isotope studies of recent sediments (Staubwasser et al. 2006) and soils (Wiederhold et al. 2007a, 2007b, Guelke et al. 2010), but the full sequential scheme has not previously been applied to Fe isotope studies. The PC-Method includes a separate chromous chloride reduction of FeS_2, but this technique extracts other Fe phases as well, and is also unsuitable for Fe isotope analysis because of a mass interference of ^{54}Cr on ^{54}Fe, which cannot be corrected for if Cr is present above typical blank concentrations during mass spectrometry. A better method for extracting silicates (with HF) and pyrite (HF-insoluble residue) was developed by Huerta-Diaz and Morse (1990) and adopted for iron

120 isotope analysis by Severmann et al. (2006). This approach may be used subsequently to the
121 extraction protocol shown here, to determine the isotopic composition of pyrite Fe.

122

123

124 **2 Method development and testing**

125 **2.1 Extraction of Fe phases (PC-Method)**

126 Leaching is generally started with 5 mL of 1 M Na-acetate (adjusted to pH 4.5 with
127 acetic acid) per ~50 mg of sediment for 24 h under an Ar-atmosphere. This extraction step
128 targets carbonate-associated Fe (Tessier et al. 1979, Poulton and Canfield 2005), but also
129 removes AVS (Cornwell and Morse 1987, Poulton and Canfield 2005) and surface-reduced
130 Fe(II) (Crosby et al. 2005, 2007). In the second step, 5 mL of 1 M hydroxylamine-HCl in 25%
131 v/v acetic acid (Chester and Hughes 1967) are reacted with the residue for 48 h. This step
132 targets easily reducible Fe oxide minerals such as ferrihydrite and lepidocrocite (Poulton and
133 Canfield 2005). Leaching is then continued with a 2 h treatment of 5 mL of Na-dithionite (50
134 g L^{-1})/Na-citrate solution (pH 4.8) (Mehra and Jackson 1960, Lord III 1980). Compared to
135 Canfield (1989) and Poulton and Canfield (2005) we used less citrate (0.02 M instead of 0.2
136 M) in order to lower the risk of matrix effects during MC-ICP-MS measurements. Citrate is
137 commonly added as a complexing agent in excess to complex Fe(II) in solution. We ensured
138 the stability of Fe in solution by performing this extraction step under anoxic conditions and
139 observed total dissolution of a goethite-hematite mineral standard (see below) and no re-
140 precipitation of Fe (oxyhydr)oxides. The sequential extraction is completed by leaching with
141 0.2 M ammonium oxalate/0.17 M oxalic acid for 6 h to dissolve magnetite. After each
142 extraction step samples were centrifuged and the supernatants filtered through 0.2 µm
143 polyethersulfone filters.

2.2 Preparation of leachate solutions for isotope analysis

The PC-Method was modified to accommodate the requirements for $\delta^{56}Fe$ isotope analysis, where the main problem is uncorrectable matrix-induced bias of measured isotope ratios. Procedures were developed to remove the leaching chemicals prior to standard column chromatography and mass-spectrometric methods (see below). The matrix removal and the accuracies of isotope ratios were verified by reference samples of known composition. These were a) 0.5 mL of an iron standard solution (1000 ppm Fe Certipur®) to which for each leaching step the appropriate chemicals were added and subsequently removed, and b) a hematite-goethite mixture prepared according to Cornell and Schwertmann (1996) ($\delta^{56}Fe$: 0.26±0.03‰, see Staubwasser et al. 2006), which was used for the dithionite extraction step only. These and all other subsequent (natural and artificial) samples were processed as follows:

Acetate extraction, (Fe_{aca}): After centrifugation and filtration the acetate matrix was destroyed by repetitive oxidation in a mixture of distilled HNO_3 and HCl (1:3) with additional H_2O_2 (supra pure grade) (see below for reproducibility of $\delta^{56}Fe_{Fe_{aca}}$ data). The complete procedure for matrix removal is shown in Figure 1. Iron was precipitated from the solution as Fe hydroxide (Fig. 1) to ensure complete separation from matrix. (Centrifuging the samples at 4°C helps to keep the Fe precipitate at the bottom of the test tube.) Subsequently, column chromatography was performed using the BioRad AG® 1-X8 anion exchange resin (Strelow 1980), as described by Schoenberg and von Blanckenburg (2005).

Hydroxylamine-HCl extraction (Fe_{hyam}): Filtered samples were repetitively oxidized and re-dissolved in 6 M HCl before column separation was performed as described for the previous extraction step (Fig. 1).

Na-dithionite/Na-citrate extraction ($Fe_{di\text{-}ct}$): Samples were oxidized (Fig. 1) and after evaporation, residues were heated for >7 h at 190°C for thermal destruction of the citrate. Afterwards, H_2O_2 and *aqua regia* were carefully added to the samples to oxidize the reduced sulfur species in the remaining dithionite to SO_4^{2-}. Subsequent iron hydroxide precipitation (Fig. 1) was performed to remove all Fe from the sulfate matrix which would otherwise overload the anion exchange resin. Furthermore, iron precipitation showed whether citrate was fully removed from the solution, whereby incomplete iron precipitation was indicated by a yellowish supernatant color due to citrate remaining in the solution. In this case, thermal heating was repeated. Further processing of the samples for column chromatography was performed as described above.

Oxalic acid extraction (Fe_{oxa}): The filtrate was oxidized and after evaporation, samples were heated for 24 h at 140°C to further oxidize the oxalate to CO_2 (Fig. 1). During heating, oxalate crystals condensating at the rim of the beakers were flushed back with ultra-pure water. Residues were re-dissolved in *aqua regia* and H_2O_2 (Fig. 1). After boiling (2 h at 120°C) and evaporation, iron precipitation and sample preparation for column chromatography was performed as described above. Iron precipitation was performed to ensure the completeness of oxalate removal. When Fe precipitation was inhibited, heating of the sample for oxalate destruction was repeated.

2.3 MC-ICP-MS setup

Prior to mass-spectrometry, concentrations of leached sediment samples were matched to 1 ppm following ICP-OES analysis (Spectro Arcos ICP-OES). Iron isotope measurements were performed on a ThermoFinnigan Neptune MC-ICP-MS instrument at the Steinmann Institute in Bonn following the method described by Schoenberg and von Blanckenburg (2005). ^{53}Cr and ^{60}Ni were simultaneously measured to monitor interferences of ^{54}Cr on ^{54}Fe and ^{58}Ni on ^{58}Fe, and the data corrected accordingly. We used the standard-sample bracketing method with the IRMM-014 standard. An in-house standard (Johnson&Matthey, Fe Puratronic wire, $\delta^{56}Fe$ = 0.42±0.05‰) was additionally measured every 6 samples to monitor accuracy. Pore-water samples were matched to 0.2 ppm and measured using an ESI Apex-Q desolvator instead of the regular glass spray chamber.

Data are reported as

$$\delta^{56}Fe\ [‰] = [(^{56}Fe/^{54}Fe_{sample}) / (^{56}Fe/^{54}Fe_{IRMM\text{-}014}) - 1] * 1000$$

Iron isotope fractionation between two species X and Y are given as

$$\Delta^{56}Fe_{X\text{-}Y} = \delta^{56}Fe_X - \delta^{56}Fe_Y$$

2.4 Procedure blanks, accuracy and reproducibility of $\delta^{56}Fe$ data leached from sediment samples

Recoveries of the Certipur® Fe standards were between 83 and 101% for all extractants, when normalized to the unprocessed standard solution (Table 1). The amount of Fe in the standards (0.5 mg) was higher, but in the same order of magnitude as that extracted from sediments. The low recoveries for oxalate are due to loss of material during the sometimes vigorous oxidation reaction. Reagent blanks were 1.2 ng mL^{-1} for Na acetate solution, 43 ng mL^{-1} for hydroxylamine-HCl, 54 ng mL^{-1} for dithionite-citrate, and 4.1 ng mL^{-1} for oxalate. Processing blanks that were added in between sediment samples had between

0.1 and 0.4 µg Fe (Table 1) and were thus two to three orders of magnitude lower than Fe contents of natural samples. Three out of 33 blanks were clearly contaminated (Grubb's outlier test, α=0.05) and therefore eliminated from calculations. Contamination concerned oxalate samples and may have happened during the thermal destruction step.

The Certipur® standards that underwent chemical processing were isotopically identical within error to the unprocessed solution (δ^{56}Fe = 0.15±0.03‰, n=9). Values for the extractants were: 0.14±0.03‰ for acetate (n=7), 0.13±0.02‰ for hydroxylamine-HCl (n=5), 0.09±0.03‰ for dithionite-citrate (n=7), and 0.14±0.04‰ for oxalate (n=5) (Fig. 2). The reproducibility of our internal Certipur® standard, regardless of whether it was subjected to the extraction steps of the PC-Method or not, suggests that the process that led to the loss of Fe during processing of the samples did not result in a significant fractionation of Fe isotopes.

The hematite-goethite standard was also dissolved in HCl/HNO_3 and measured without further chemical treatment, except for the column separation. This gave a δ^{56}Fe composition of 0.27±0.01‰ (1SD, n=3, Fig. 2). The δ^{56}Fe value of the dithionite-leached and fully processed mineral standards was 0.30±0.07‰ (n=5) compared to 0.26±0.03‰ given by Staubwasser et al. (2006) (n=11). These data demonstrate the absence of matrix-induced bias in Fe isotope ratios in samples leached and subsequently processed by the methods outlined in this study.

2.5 Selectivity of the Fe extraction steps

2.5.1 Materials and set-up of experiments

234 *Time resolved leaching rate experiments:* Using synthetic minerals, the selectivity of the
235 chemical extractions by Na-acetate, hydroxylamine-HCl, and Na-dithionite/Na-citrate was
236 evaluated. This is important, as dependent on the size of Fe pools and their isotopic
237 differences, non-selectivity of the leaching can lead to incorrect Fe isotope values for the
238 actual target fraction. The minerals were synthesized after Cornell and Schwertmann (1996).
239 About 5 mg of the specific Fe oxide was suspended in 50 mL of an extraction solution not
240 designed to lead to its dissolution: ferrihydrite was treated with Na-acetate for 12, 24, 36,
241 48, and 60 h, goethite and hematite were treated with hydroxylamine-HCl for 12, 24, 36, 48,
242 and 60 h, and magnetite was treated with Na-dithionite/Na-citrate for 1, 2, and 4 h. In
243 contrast to earlier studies (Canfield 1988, Raiswell et al. 1994, Poulton and Canfield 2005)
244 magnetite was significantly dissolved by dithionite treatment (see below) and the leaching
245 was thus repeated using magnetite purchased from Alfa Aesar. Although not used on natural
246 samples in this study, we also evaluated 0.5 M HCl extraction that targets poorly crystalline
247 hydrous ferric oxides such as ferrihydrite (Kosta and Luther 1994, Severmann et al. 2006).
248 The synthetic minerals ferrihydrite, goethite, hematite, and magnetite were subject to 0.5 M
249 HCl for 0.5, 1, 2, 4, and 8 h at room temperature. After each time step, the respective
250 samples were centrifuged and aliquots of 15 mL were filtered. Na-acetate, hydroxylamine-
251 HCl, and dithionite samples were processed as described above, but omitting Fe
252 precipitation and column chromatography as only Fe concentrations were to be obtained.
253 The processing of HCl-samples was reduced to evaporation and subsequent re-dissolution in
254 0.3 M HNO_3 prior to Fe concentration measurement by ICP-OES.

255 *Leaching of pairs of isotopically spiked and non-spiked minerals:* Mixtures of two synthetic
256 minerals were treated with extractants (hydroxylamine-HCl, Na-dithionite, and 0.5 M HCl) to
257 test the selectivity of the leaching steps. The respective target mineral was mixed with a

^{58}Fe-spiked non-target mineral (e.g. non-spiked ferrihydrite plus spiked goethite for hydroxylamine-HCl extraction). Based on the aforementioned observation of our magnetite minerals significantly dissolving in dithionite solution, additional tests with magnetite purchased from Alfa Aesar (non-spiked) were performed with spiked goethite and hematite, respectively. To allow for the high iron concentrations when using pure phases compared to natural sediment samples, about 10 mg of the synthetic minerals (5 mg spiked mineral + 5 mg non-spiked mineral) was treated with 50 mL of the respective leaching reagent (in contrast to 50 mg + 5 mL for sediment samples, see above). For each mineral pair, three replicates were processed. After centrifugation, 15 mL of the extract was filtered for further processing for Fe isotope analysis as described above. Dissolution of target and non-target minerals was evaluated by comparing ^{58}Fe/^{54}Fe ratios of the leachates with those of the respective pure synthetic minerals. The latter ratios were determined after dissolution of the pure minerals in *aqua regia*, evaporation, re-dissolution in 6 M HCl, and column chromatography.

2.5.2 Selectivity of extraction steps

Time resolved leaching rate experiments: With the exception of the dithionite extraction, the treatment of synthetic Fe (oxyhydr)oxide minerals with reagents that are commonly used in the subsequent extraction step led to only minor dissolution, verifying the results of Poulton and Canfield (2005). As expected, mineral dissolution increased with the duration of leaching (Fig. 3). At optimum times for acetate- and hydroxylamine-HCl extractions (according to the PC-Method), less than 1% of the non-target minerals ferrihydrite and goethite + hematite, respectively, were dissolved. Carry-over of ferrihydrite-Fe into the Na-acetate fraction was 0.3% compared to 1.7% given by Poulton and Canfield

(2005) and can thus be considered insignificant. The slightly higher dissolution of hematite in hydroxylamine-HCl compared to goethite could be related to grain-size differences and also the degree of crystallinity of the hematite (freshly-precipitated hematite is more readily dissolved than natural hematite; Raiswell et al. 1994). With respect to iron isotope signatures, a carry-over of <1% of goethite- and hematite-Fe into the fraction of amorphous Fe is, however, insignificant for typical marine or fluvial sediments as Fe_{hyam} and $Fe_{di\text{-}ct}$ concentrations usually range in the same order of magnitude.

We observed considerable dissolution of magnetite in Na-dithionite/Na-citrate for both the magnetite synthesized after Cornell and Schwertmann (1996) and the magnetite purchased from Alfa Aesar. The 2 h-treatment led to dissolution of up to 50% of the magnetite (Fig. 3), which is in contrast to the results of Poulton and Canfield (2005) who observed dissolution of only up to 7%, and Raiswell et al. (1994) who observed only 4% dissolution. In our study the significant difference in dissolution of the magnetite produced after Cornell and Schwertmann (1996) and the purchased magnetite (52% vs. 32% after 2 h in dithionite/citrate) indicates that grain size might considerably affect dissolution. However, the magnetite synthesized after Cornell & Schwertmann was similar to that used by Poulton and Canfield (2005) and yet was strongly dissolved. Interestingly, Kostka and Luther (1994) also observed significant magnetite dissolution in dithionite (90.2%). The authors, however, leached for 4 h at 60°C, so their data are not directly comparable to previous studies. The disparity in our data relative to previous studies was possibly caused by differences in sample size used per volume of solution, crystallinity, or potentially by partial oxidation of magnetite during storage. The 1 h extraction by 0.5 M HCl resulted in effective dissolution of ferrihydrite (>95%) while goethite, hematite, and magnetite remained largely unaffected (Fig. 3).

306 *Leaching of pairs of isotopically spiked and non-spiked minerals*: Test results of
307 experiments with ^{58}Fe spiked and non-spiked minerals are shown in Table 2. The $^{58}Fe/^{54}Fe$
308 ratios of samples and pure minerals as end-members are given in the appendix (Tables A.1
309 and A.2). In accordance with the previous time-resolved experiment, the isotopic data of
310 leached mineral mixtures demonstrate that goethite and hematite remain unaffected by the
311 hydroxylamine-HCl extraction. For both pairs (each with ferrihydrite), 98% of the dissolved
312 Fe in solution was derived from ferrihydrite and ~2% originated from goethite and hematite.
313 In hydroxylamine-HCl, 87% of the ferrihydrite-Fe was recovered, which is slightly less than
314 the 99% given by Poulton and Canfield (2005). Dithionite effectively dissolved goethite and
315 hematite. In the first experiment, where minerals have been mixed with ^{58}Fe-spiked
316 magnetite synthesized after Cornell and Schwertmann (1996), ~96% of goethite and
317 hematite were dissolved after 2 h. In the repeated run with magnetite from Alfa Aesar,
318 recoveries were, however, lower (79 to 88%; Table 2). In both runs, magnetite was
319 significantly dissolved and data produced by the mixing experiment match those of the
320 single mineral extraction: Dithionite extracted up to 50-60% of our synthetic magnetite and
321 30-40% of the Alfa Aesar magnetite.
322
323 **3 Application of the new method to surface sediments of the North Sea**
324 **3.1 Material and methods**
325 **3.1.1 Core location and sampling**
326 Data presented in this study were obtained for surface sediments retrieved by a
327 multicorer in the German Bight (North Sea, 54°5.06' N, 7°54.94' E, 36 m water depth; site
328 HE337-1) in 2010 during cruise HE337 of research vessel HEINCKE. The sediment cores were
329 collected west of the so-called Helgoland mud area, one of the few depocenters of fine-

grained sediments in the North Sea with eddy focusing of fine-grained material from the rivers Weser and Ems (Hertweck 1983). Sedimentation rates in the Helgoland mud area are ~2.6 mm/yr for the last 750 years (Hebbeln et al. 2003). The location was chosen as sediments exhibit an extended ferruginous zone starting directly below the sediment surface in contrast to deposits within the Helgoland mud area proper, where the upper iron reduction zone is limited to the upper 15 cm (Oni et al. 2015). At the core location, bioturbation (and potentially bioirrigation) occur. However, the generally rather undisturbed pore-water profiles suggest that these processes proceed at a comparatively low rate (see section 3.2).

Sediment analyses performed on one core included the sequential iron extractions of the PC-Method for iron concentration and iron isotope analysis, bulk sediment total acid digestion for total Al, Mn, and Fe (Fe_{total}) contents, in addition to AVS and pyrite-sulfide extraction after Canfield et al. (1986) (without subsequent Fe isotope analysis). Sediment was sampled directly on board using syringes with cut tips. The syringes were sealed and stored in Ar-filled gas-tight glass containers at -20°C until processing to prevent secondary mineral precipitation. Pore-water was sampled from a parallel core using rhizons (Seeberg-Elverfeldt et al. 2005, Dickens et al. 2007) that were inserted into pre-drilled holes in the liner. In order to inhibit oxidation during sampling, due to O_2 in either the rhizon or the attached syringe, the rhizons were pre-soaked with ultra-pure water and the first 0.5 mL or pore-water was discarded. Pore-water aliquots for $\delta^{56}Fe_{Fe(II)_{aq}}$ were acidified with double distilled HCl and stored in pre-cleaned vials at 4°C.

3.1.2 Sequential Fe extraction (PC-Method)

353 Sediment samples were leached in random order. About 50 mg of freeze-dried
354 sediment was washed with 5 mL of 1 M $MgCl_2$ for 2 h in order to remove pore-water
355 constituents, which will also have removed exchangeable ions on particle surfaces (Tessier et
356 al. 1979, Poulton and Canfield 2005). The $MgCl_2$ washing was performed under an Ar
357 atmosphere to prevent oxidation. The residue was then used for the subsequent extraction
358 steps (see chapter 2.1). The extraction solutions were processed as described in sections 2.2
359 and 2.3.

360

361 **3.1.3 Bulk sediment composition**

362 Total acid digestion of sediment samples was performed with a CEM Mars Xpress
363 microwave system using ~50 mg of freeze-dried sediment and a mixture of HNO_3 (3 mL), HCl
364 (2 mL), and HF (0.5 mL). With each set of samples, blanks and standard reference material
365 (NIST SRM 2702) were processed. Element concentrations were measured by ICP-OES (Iris
366 Intreprid II). Recoveries of the standard were 97.5% for Al, 100.4% for Fe, and 98.9% for Mn.

367

368 **3.1.4 AVS- and pyrite-S**

369 Acid volatile sulfide and pyrite were determined for the North Sea sediments to both
370 correct the Na-acetate leached Fe pool for the presence of AVS, and to assess the extent of
371 early diagenetic iron transformation at the study site. Extractions (after Canfield et al. 1986)
372 with HCl (for AVS) and chromous chloride distillation (for pyrite) were performed at the
373 University of Leeds. These extractions determine the concentration of sulfide present, which
374 is then stoichiometrically converted to the appropriate Fe concentration. Replicates of three
375 samples (each analyzed 2-4 times) revealed good reproducibility with a RSD of below 5% in

all cases. Accuracy was evaluated by analysis of an in-house standard (HN22) with a pyrite-Fe content of 2.12 ± 0.16 wt% (our measured value: 2.18 wt%).

3.1.5 Pore-water composition

On board pore-water analyses comprised the determination of $Fe(II)_{aq}$ using the ferrozine method of Stookey (1970) and of alkalinity by titration with HCl (see appendix A.3 for alkalinity). Offshore measurements of SO_4^{2-} were performed as described by Henkel et al. (2012). Pore-water Fe for $\delta^{56}Fe_{Fe(II)_{aq}}$ analysis was concentrated and purified from anions using NTA Superflow (Lohan et al. 2005). The acidified samples were titrated with NH_4OH (supra pure grade) to a final pH of 2. In order to oxidize Fe(II) to Fe(III), 10 µM H_2O_2 was added to the samples before loading of NTA Superflow columns (Qiagen). The NTA columns were pre-conditioned with HCl (pH2, HCl triple distilled). Fe was subsequently eluted using 1 M HCl. The samples were further purified by anion exchange chromatography as described in section 2.2 and measured by MC-ICP-MS (see section 2.3).

3.2 Results and discussion

3.2.1 Geochemical results

Geochemical data gained for Site HE337-1, including Fe phases and pore-water constituents are shown in Figures 4 and 5 (note that Fe_{aca}* has been corrected for Fe_{AVS} and that Fe_{AVS} was a minor constituent of Fe_{aca} in our samples; Figure 5). Total Fe contents range between 1.9 and 4.6 wt%. Unsulfidized reactive iron (Fe_{unsulf} =Fe_{aca}*+ Fe_{hyam} + $Fe_{di\text{-}ct}$ + Fe_{ox}) varies between 0.5 and 1.0 wt% (Fig. 4). Although Fe_{unsulf} remains relatively constant with depth, a decrease in Fe_{unsulf} relative to Fe_{total} is observed with depth through the top 10 cm

399 of the sediment. At the core top, Fe_{hyam} represents about 50% of the unsulfidized Fe pool,
400 and when normalized to Fe_{unsulf}, shows an overall decrease to ~20 cm depth (Fig. 5). Fe_{aca}
401 and $Fe_{di\text{-}ct}$ amount to ~20 and ~30% of Fe_{unsulf}, respectively. Whereas Fe_{aca}/Fe_{unsulf} generally
402 increases towards 20 cm depth, with a subsequent overall decrease below, albeit with
403 significant variability at certain horizons, $Fe_{di\text{-}ct}/Fe_{unsulf}$ does not show a clear trend with
404 depth. Fe_{oxa} is of minor importance, contributing only ~10% to the Fe_{unsulf} pool throughout
405 most of the core, perhaps with a slight increase in Fe_{oxa}/Fe_{unsulf} over the top 10 cm.
406 Regarding the generally lower amount of Fe_{oxa} compared to $Fe_{di\text{-}ct}$ in this core, we consider
407 the effect of any possible magnetite dissolution in the $Fe_{di\text{-}ct}$ extract as being minor.

408 Sulfide-bound Fe is mainly present as pyrite (Fig. 5) with an increase towards 15 cm
409 depth. The Fe_{AVS} pool is relatively insignificant, with highest contents of 0.02 wt% at 18 cm
410 depth. Manganese oxide reduction is evidenced by a pronounced Mn/Al decrease in the top
411 3 cm (Fig. 4). Pore-water profiles (Fig. 4) indicate organoclastic sulfate reduction at ~7 cm
412 depth coinciding with a peak in $Fe(II)_{aq}$ (~200 µM) produced by DIR, with ferruginous pore-
413 water prevailing over the full length of the core. $\delta^{56}Fe_{Fe_{aq}}$ values are lightest (-1.3‰) at 1.5
414 and 4.5 cm depth, where DIR dominates Fe cycling. At 0.5 cm, where Fe(II) is removed from
415 solution by oxidative precipitation (as indicated by a drawdown of $Fe(II)_{aq}$), $\delta^{56}Fe_{Fe_{aq}}$ is
416 slightly heavier (-0.9‰). Below 5 cm depth (still within the $Fe(II)_{aq}$ maximum and coinciding
417 with the presence of AVS), the isotopic composition of pore-water Fe becomes heavier and
418 reaches a value of about zero at 18 cm, where $Fe(II)_{aq}$ concentrations level off to about 40
419 µM.

420 In the leached sediment fractions, a pronounced $\delta^{56}Fe$ trend with depth is observed
421 only for Fe_{aca}, with values that increase from ~-1‰ at the surface, to slightly positive values

422 at depth (Fig. 5). Fe_{hyam} shows an overall depletion in ^{56}Fe ($\delta^{56}Fe$ = -0.38±0.11‰), whereas
423 $Fe_{di\text{-}ct}$ and Fe_{oxa} show near zero values (-0.07±0.09‰ and -0.15±0.08‰, respectively).

424

425 **3.2.2 Early diagenetic iron cycling in shallow North Sea sediments**

426 The Fe phases extracted by the dithionite/citrate and oxalate solutions (goethite,
427 hematite, magnetite) are largely unaffected by DIR as concluded from the absence of clear
428 downcore trends in $Fe_{di\text{-}ct}$ and Fe_{oxa} contents and respective $\delta^{56}Fe$ profiles (Fig. 5). Near zero
429 values of $\delta^{56}Fe_{di\text{-}ct}$ and $\delta^{56}Fe_{oxa}$ reflect largely unaltered terrigenous input of these fractions
430 (e.g. Johnson et al. 2008). $Fe_{di\text{-}ct}$ and Fe_{oxa} contents vary between 0.1 to 0.3 wt% and 0.03 to
431 0.09 wt%, respectively (see appendix A.4). The downcore variability in $Fe_{di\text{-}ct}/Fe_{react}$ and
432 Fe_{oxa}/Fe_{react} is most likely related to changing depositional regimes/sediment accumulation,
433 rather than to a diagenetic overprint. As has been pointed out by Hebbeln et al. (2003), the
434 intensification of beam-trawl fishing off the German coast increased overall sediment
435 accumulation in the mud area during the 20th century and led to a coarsening of sediments.
436 These changes caused by anthropogenic activity are likely also reflected at Site HE337-1.
437 Here, west of the mud area, sedimentation rates are expected to be lower than the ~2.6
438 mm/yr in the sediment-focusing mud area (Hebbeln et al. 2003). Consequently, the retrieved
439 sediment core covers at least the past 150 yrs and thus the time when sedimentation
440 patterns changed.

441 The slight ^{56}Fe-depletion in the hydroxylamine-leachable fraction ($\delta^{56}Fe_{hyam} \approx$ -
442 0.38‰), relative to terrigenous sediments typically showing similar $\delta^{56}Fe$ values to igneous
443 rocks (~0.1‰; Beard et al. 2003b) might reflect that part of the pool was diagenetically
444 altered by precipitation of secondary amorphous Fe oxides in the (sub)oxic zone. Under

445 anoxic conditions (below 1-2 cm depth), this pool is used for DIR reflected by a decrease of
446 Fe_{hyam}/Fe_{unsulf} from 0.45 to 0.35 in the top 10 cm (Fig. 5). However, at this location, the Fe_{hyam}
447 reduction does not lead to a significant downcore trend in $\delta^{56}Fe_{hyam}$.

448 AVS was detected at 3 cm depth, suggesting that sulfidization starts at this depth,
449 which matches the slight SO_4^{2-}-drawdown (Fig. 4). Pyrite, however, is already present in the
450 surface sediment. Bioturbation might have transported iron sulfides previously formed in
451 the deeper part of the sediments towards the sediment surface. There, AVS is prone to
452 oxidation whereas pyrite is less susceptible to oxidation and survives longer before being
453 buried again into the anoxic zone.

454 The $\delta^{56}Fe_{Fe_{aq}}$ trend towards a slightly heavier value of -0.9‰ at 0.5 cm compared
455 to -1.3‰ at 1.5 cm and at 4.5 cm, where DIR dominates, is explained by oxidative
456 precipitation of Fe that preferentially removes light Fe isotopes (Staubwasser et al. 2013).
457 Since the water column above the sediment is fully oxic, Fe-oxides must precipitate at the
458 sediment surface. The oxidative layer, however, only extents to about 1 cm. Directly below,
459 DIR dominates as indicated by the low $\delta^{56}Fe_{Fe_{aq}}$. Below 5 cm, and in the sample at 3.5 cm,
460 $\delta^{56}Fe_{Fe_{aq}}$ is only -0.4‰. We suggest that at these depths, AVS formation removes light Fe
461 isotopes from solution. The sediment core was significantly bioturbated and the 3.5 cm
462 sample might reflect local AVS formation in a burrow with elevated TOC contents. Since the
463 $Fe(II)_{aq}$ profile suggests maximum rates of DIR at about 6 cm, DIR and AVS formation seem to
464 coincide at least between 3 and 6 cm depth. Below 18 cm, $\delta^{56}Fe_{Fe_{aq}}$ reaches values of about
465 zero suggesting that DIR is no longer significant and Fe diagenesis is dominated by reactions
466 with H_2S.

467

3.2.3 Acetate-leachable iron fraction

The comparatively high amounts of Fe_{aca} found at site HE337-1 (0.16±0.05 wt%) are unlikely to be due to the presence of siderite or AVS. AVS only accounts for up to 8% of the Fe_{aca} fraction. The depth of the AVS-maximum (17-21 cm), however, coincides with a local minimum in $\delta^{56}Fe_{aca}$, so the low $\delta^{56}Fe_{aca}$ values at these depths might result from dissolution of the ^{56}Fe-depleted amorphous Fe sulfides (Guilbaud et al. 2013) during the Na-acetate extraction. Siderite is generally considered rare in modern shallow organic-rich marine sediment as it is thermodynamically unstable in the presence of H_2S (Haese 2006). Organoclastic sulfate reduction is clearly occurring in these sediments, as indicated by the presence of AVS and the broad ferruginous zone. As such, even though H_2S is quantitatively removed from solution by reaction with Fe minerals (Fig. 4), siderite would not be expected to form in these sediments. Additionally, $\delta^{56}Fe_{Fe(II)_{aq}}$ data support an absence of authigenic siderite formation: Abiotic siderite precipitation is characterized by a preferential uptake of light isotopes from $Fe(II)_{aq}$. The respective fractionation factor given by Wiesli et al. (2004) is $\Delta^{56}Fe_{Fe(II)_{aq}\text{-siderite}}$ = +0.48±0.22‰. If Fe_{aca} with $\delta^{56}Fe_{Fe_{aca}}$ ranging between -1 and 0‰ (Fig. 5) was mainly derived from authigenic siderite, respective $\delta^{56}Fe_{Fe(II)_{aq}}$ values would need to be between -0.5 and 0.5‰. In the top 10 cm (where DIR dominates) $\delta^{56}Fe_{Fe(II)_{aq}}$ values are, however, light (-0.4 to -1.4‰) compared to $\delta^{56}Fe_{Fe_{aca}}$.

The Fe_{aca} extraction does not include $Fe(II)_{aq}$ as this has been removed by washing the samples with 1 M $MgCl_2$ before the sequential extraction. Without performing a washing step, $Fe(II)_{aq}$ would potentially amount to a maximum of ~20 µg/g sediment, corresponding to ~2% of the Fe_{aca} pool. The above considerations exclude siderite, AVS, and $Fe(II)_{aq}$ as forming a significant proportion of the Na-acetate leached fraction. Instead, we suggest that this pool dominantly reflects isotopically light Fe(II) adsorbed to mineral surfaces following

492 DIR (e.g. Beard et al. 2003a, Williams and Scherer 2004, Crosby et al. 2005, 2007, Mikutta et
493 al. 2009), or Fe(II) that has formed at the surface of Fe oxide minerals via direct abiotic
494 reaction with sulfide, but which dissolves only slowly from the mineral surface at
495 circumneutral pH (Poulton 2003, Poulton et al. 2004). Crosby et al. (2005, 2007) investigated
496 isotopic fractionation during DIR using synthesized goethite and hematite, and measured
497 acetate-leached $Fe(II)_{sorb}$ with negative $\delta^{56}Fe$ values resembling those of $Fe(II)_{aq}$ ($\Delta^{56}Fe_{Fe(II)_{aq}-}$
498 $_{Fe(II)_{sorb}}$=-0.87±0.09‰ and -0.30±0.08‰ for goethite and hematite, respectively). $Fe(II)_{sorb}$
499 derives from ^{56}Fe-depleted pore-water and undergoes electron transfer and Fe(II)-Fe(III)
500 atom exchange with a reactive Fe(III) layer on the ferric substrate (Williams and Scherer
501 2004; Crosby et al. 2005, 2007). The oxide surface becomes more and more enriched in ^{56}Fe
502 balancing out the light $Fe(II)_{aq}$ (Crosby et al. 2005, 2007). $Fe(II)_{sorb}$ thus represents an
503 intermediate between the light $Fe(II)_{aq}$ and isotopically heavy reactive Fe(III). The natural
504 sediments investigated here represent a mineralogically much more complex environment.
505 Nevertheless, we observe trends that resemble those shown in laboratory studies. Therefore
506 we suggest that the underlying processes observed are the same and the light $\delta^{56}Fe$ values
507 we measure for the Fe_{aca} pool likely dominantly reflect Fe(II) at the mineral surface that is
508 fractionated by coupled electron and atom exchange.

509 Our data show variations in $\Delta^{56}Fe_{Fe_{aca}-Fe_{hyam}}$ of between -0.7 to 0.6‰, which is distinct
510 from the fractionation factors found by Crosby et al. (2007). Their $\Delta^{56}Fe_{Fe(II)_{sorb}-Fe(III)_{react}}$ is
511 ~-1.75‰ for goethite and -2.65‰ for hematite experiments. However, the processes at our
512 study site take place in an open system with diffusive $Fe(II)_{aq}$ transport, preferential removal
513 of ^{54}Fe from $Fe(II)_{aq}$ by sulfide precipitation, and non-controlled exposure times of ferric
514 minerals to $Fe(II)_{aq}$. In this regard, and due to the fact that Crosby´s fractionation factors only

correspond to the reactive Fe(III) layer (not to the whole ferric substrate), the fractionation factors are not directly comparable.

The $\delta^{56}Fe$ measurements suggest that of the unsulfidized solid phase Fe pools in modern DIR-dominated marine sediments, the acetate-leachable pool is the most dynamic. A sequential extraction for marine sediments that uses acetate as a first step followed by hydroxylamine-HCl or 0.5 M HCl leaching is thus to be preferred over leaching with Na-dithionite alone. Leaching by Na-dithionite dissolves a mixture of Fe fractions that are otherwise distinct in origin, reactivity, and isotopic composition and does not selectively resolve the pools truly affected by DIR. Similarly, extractions using 0.5 M HCl alone (i.e. not including the Fe_{aca} extraction first) dissolve the total "easily reducible" Fe fraction, which mainly includes three isotopically distinct Fe pools: the light Fe_{aca} pool that has been shown here to mainly comprise surface-reduced Fe(II), unaltered poorly crystalline hydrous ferric oxides such as ferrihydrite, and ^{56}Fe-enriched reactive Fe at the oxide surface (as identified by Williams and Scherer 2004 and Crosby et al. 2005, 2007). Interpretation of the acetate fraction and its isotopic composition, however, can be problematic where a discrimination between AVS-Fe, surface-reduced Fe(II), and siderite is not possible and where pore-water $\delta^{56}Fe$ data are not available.

4 Conclusions

We have developed a procedure to complement an existing sequential extraction method for Fe phases in marine sediment, to enable stable Fe isotope analysis on the leachates. Processing of the samples for matrix removal did not lead to significant Fe isotope fractionation. This new method was applied to surface sediments collected from the southern North Sea that showed an extended ferruginous pore-water zone. In general, the

539 different $\delta^{56}Fe$ values of individual reactive Fe pools demonstrates their different genetic
540 origin: ferrihydrite/lepidocrocite showed lowest average $\delta^{56}Fe$ values (-0.38±0.11‰) as they
541 likely include authigenic/secondary phases originating from light $Fe(II)_{aq}$ released into the
542 pore-water by DIR. The detrital origin of the goethite/hematite and magnetite fractions was
543 indicated by $\delta^{56}Fe \approx 0‰$. Goethite, hematite, and magnetite were not considerably involved
544 in early diagenetic Fe cycling at this locality. The $\delta^{56}Fe$ data show large downcore $\delta^{56}Fe$
545 variations in the acetate-leachable fraction. This trend could not be explained by AVS-Fe as
546 respective concentrations were too low. Furthermore, diagenetic siderite was excluded as a
547 significant contributor to the acetate-leachable fraction. We conclude that in these
548 sediments the Na-acetate extraction dominantly comprises surface-reduced Fe(II) which
549 shows a downcore isotopic trend similar to that for $Fe(II)_{aq}$. Although more complex to
550 interpret based on the variety of processes that occur in natural sediments, our data are
551 consistent with the previous laboratory results of Crosby et al. (2005, 2007), who showed
552 that $Fe(II)_{sorb}$ is (isotopically) an intermediate between $Fe(II)_{aq}$ and the ferric substrate.
553 Leaching sediments by 0.5 M HCl or Na-dithionite alone would not resolve this. With
554 extraction by 0.5 M HCl, the isotopically light Fe(II) would be collected together with the
555 ^{56}Fe-enriched reactive Fe(III) layer at the mineral-surface and the unfractionated initial ferric
556 substrate. The combination of sequential Fe extractions and subsequent $\delta^{56}Fe$ analyses as
557 performed in this study represents an approach that can be useful for a broad range of
558 scientific questions in ancient and modern environments characterized by severe redox
559 changes or where control mechanisms for mineral formation (biotic vs. abiotic) are not fully
560 understood.
561

Acknowledgments: We thank J. Scheld, M. Harak, and J. Menges for assistance in the laboratory at the University of Cologne and appreciate the help of Ingrid Stimac (Alfred Wegener Institute) concerning sulfate measurements and assistance during total digestion of bulk sediments. R. Guilbaud is thanked for giving support during AVS and pyrite determinations at the University of Leeds. X-ray diffractions of synthetic minerals were performed by P. Held (University of Cologne). We further acknowledge F. Wombacher for support concerning MC-ICP-MS at the Steinmann Institute in Bonn and Alison McAnena for producing synthetic minerals. Finally, we thank Jeremy Owens and an anonymous reviewer for helpful comments on the manuscript. This study was funded by the German Research Foundation (DFG) within Priority Program 1158 "Antarctic Research with Comparable Investigations in Arctic Sea Ice Areas" and is associated to the IMCOAST project (Impact of climate induced glacial melting on marine coastal systems in the western Antarctic Peninsula region) (grant numbers STA 936/5-1 and KA 2769/3-1). We acknowledge additional funding by the Helmholtz Association (Alfred Wegener Institute, Helmholtz Centre for Polar and Marine Research) in the framework of the research programs PACES I and PACES II. Data of this study are available via the Pangaea database.

References

Anbar, A.D. and O. Rouxel (2007) Metal stable isotopes in paleoceanography. Annual Review of Earth and Planetary Sciences 35, 717–746.

Beard, B.L., C.M. Johnson, J.L. Skulan, K.H. Nealson, L. Cox, and H. Sun (2003a) Application of Fe isotopes to tracing the geochemical and biological cycling of Fe. Chemical Geology 195, 87–117.

585 Beal, E.J., C.H. House, and V.J. Orphan (2009) Manganese- and iron-dependant marine
586 methane oxidation. Science 325, 184-187.
587 Beard, B.L., C.M. Johnson, K.L. Von Damm, and R.L. Poulson (2003b) Iron isotope constraints
588 on Fe cycling and mass balance in oxygenated Earth oceans. Geology 31, 629-632.
589 Canfield, D.E., R. Raiswell, J.T. Westrich, C.M. Reaves and R.A. Berner (1986), The use of
590 chromium reduction in the analysis of reduced inorganic sulfur in sediments and shales.
591 Chemical Geology 54, 149–155.
592 Canfield, D.E. (1988) Sulfate reduction and the diagenesis of iron in anoxic marine
593 sediments. Ph.D. thesis. Yale University, 248 pp.
594 Canfield, D.E. (1989) Reactive iron in marine sediments. Geochimimica et Cosmochimica
595 Acta 53(6), 619–632.
596 Canfield, D.E., R. Raiswell, and S. Bottrell (1992) The reactivity of sedimentary iron minerals
597 towards sulfide. American Journal of Science 292, 659–683.
598 Chester, R. and M.J. Hughes (1967) A chemical technique for the separation of ferro-
599 manganese minerals, carbonate minerals and adsorbed trace elements from pelagic
600 sediments. Chemical Geology 2, 249–262.
601 Conway, T.M. and S.G. John (2014) Quantification of dissolved iron sources to the North
602 Atlantic Ocean. Nature 511, 212–215.
603 Cornell, R.M. and U. Schwertmann (1996) The iron oxides: structure, properties, reactions,
604 occurrences and uses. VCH Publishers, Weinheim, Germany.
605 Cornwell, J.C. and J.W. Morse (1987) The characterization of iron sulfide minerals in anoxic
606 marine sediments. Marine Chemistry 22, 193–206.

607 Crosby, H.A., C.M. Johnson, E.E. Roden, and B.L. Beard (2005) Coupled Fe(II)-Fe(III) electron
608 and atom exchange as a mechanism for Fe isotope fractionation during dissimilatory iron
609 oxide reduction. Environmental Science and Technology 39, 6698–6704.
610 Crosby, H.A., E.E. Roden, C.M. Johnson, and B.L. Beard (2007) The mechanism of iron isotope
611 fractionation produced during dissimilatory Fe(III) reduction by *Shewanella putrefaciens*
612 and *Geobacter sulfurreducens*. Geobiology 5, 169–189.
613 Dickens, G.R., M. Kölling, D.C. Smith, L. Schnieders, and the IODP Expedition 302 Scientists
614 (2007) Rhizon sampling of pore waters on scientific drilling expeditions: An example from
615 the IODP Expedition 302, Arctic Coring Expedition (ACEX). Proc. IODP Scientific Drilling 4,
616 doi:10.22 04/iodp.sd.4.08.2007.
617 Egger M., O. Rasigraf, C.J. Sapart, T. Jilbert, M.S.M. Jetten, T. Röckmann, C. van der Veen, N.
618 Bândă, B. Kartal, K.F. Ettwig, and C.P. Slomp (2015) Iron-mediated anaerobic oxidation of
619 methane in brackish coastal sediments. Environmental Science and Technology 49, 277-
620 283.
621 Ferdelman, T.G. (1988) The distribution of sulfur, iron, manganese, copper, and uranium in a
622 salt marsh sediment core as determined by a sequential extraction method. Master thesis,
623 University Delaware.
624 Guelke, M., F. von Blanckenburg, R. Schoenberg, M. Staubwasser, and H. Stuetzel (2010)
625 Determining the stable Fe isotope signature of plant-available iron in soils. Chemical
626 Geology 277, 269–280.
627 Guilbaud, R., I.B. Butler, and R.M. Ellam (2013) Abiotic pyrite formation produces a large Fe
628 isotope fractionation. Science 332, 1548–1551.
629 Haese, R.R. (2006) The Biogeochemistry of Iron. In: Schulz H.D., Zabel, M. (editors) Marine
630 Geochemistry. Berlin, Springer-Verlag, 207–240.

631 Haese, R.R., K. Wallmann, A. Dahmke, U. Kretzmann, P.J. Müller and H.D. Schulz (1997) Iron
632 species determination to investigate early diagenetic reactivity in marine sediments.
633 Geochimica et Cosmochimica Acta 61(1), 63–72.
634 Hebbeln, D., C. Scheurle, and F. Lamy (2003) Depositional history of the Helgoland mud area,
635 German Bight, North Sea. Geo-Marine Letters 23, 81–90.
636 Henkel, S., J.M. Mogollón, Kerstin Nöthen, C. Franke, K. Bogus, E. Robin, A. Bahr, M.
637 Blumenberg, T. Pape, R. Seifert, C. März, G.J. de Lange, and S. Kasten (2012) Diagenetic
638 barium cycling in Black Sea sediments – A case study for anoxic marine environments.
639 Geochimica et Cosmochimica Acta 88, 88–105.
640 Hertweck, G. (1983) Das Schlickgebiet in der inneren Deutschen Bucht. Aufnahme mit dem
641 Sedimentechographen. Senckenbergiana marit 15, 219–249.
642 Homoky, W.B., S. Severmann, R.A. Mills, P.J. Statham, and G.R. Fones (2009) Pore-fluid Fe
643 isotopes reflect the extent of benthic Fe redox recycling: Evidence from continental shelf
644 and deep-sea sediments. Geology, 37(8), 751–754.
645 Homoky, W.B., S.G. John, T.M. Conway, and R.A. Mills (2013) Distinct iron isotopic signatures
646 and supply from marine sediment dissolution. Nature Communications, 4:2143.
647 Huerta-Diaz, M. and J.W. Morse (1990) A quantitative method for determination of trace
648 metal concentrations in sedimentary pyrite. Marine Chemistry 29, 119–144.
649 Hyacinthe, C. and P. van Cappellen (2004) An authigenic iron phosphate phase in estuarine
650 sediments: composition, formation and chemical reactivity. Marine Chemistry 91, 227–251.
651 Jensen, M.M., B. Thamdrup, S. Rysgaard, M. Holmer, and H. Fossing (2003) Rates and
652 regulation of microbial iron reduction in sediments of Baltic-North Sea transition.
653 Biogeochemistry 65, 295–317.

654 Johnson, C.M, B.L. Beard, and E.E. Roden (2008) The iron isotope fingerprints of redox and
655 biogeochemical cycling in modern and ancient Earth. Annual Review of Earth and Planetary
656 Sciences 36, 457–493.
657 Kasten, S., T. Freudenthal, F.X. Gingele, and H.D. Schulz (1998) Simultaneous formation of
658 iron-rich layers at different redox boundaries in sediments of the Amazon deep-sea fan
659 Geochimica et Cosmochimica Acta 62(13), 2253–2264.
660 Kostka, J.E. and G.W. Luther (1994) Partitioning and speciation of solid iron in saltmarsh
661 sediments. Geochimica et Cosmochimica Acta 58, 1701–1710.
662 Lohan, M.C., A.M. Aguilar-Islas, R.P. Franks and K.W. Bruland (2005) Determination of iron
663 and copper in seawater at pH 1.7 with a new commercially available chelating resin, NTA
664 Superflow. Analytica Chimica Acta 530, 121–129.
665 Lord III, C.J. (1980) The chemistry and cycling of iron, manganese and sulfur in a salt marsh
666 sediment, Dissertation thesis, University of Delaware.
667 März, C., J. Hoffmann, U. Bleil, G.J. de Lange, and S. Kasten (2008) Diagenetic changes of
668 magnetic and geochemical signals by anaerobic methane oxidation in sediments of the
669 Zambezi deep-sea fan (SW Indian Ocean). Marine Geology 255, 118-130.
670 McKeague, J.A. and J.H. Day (1966) Dithionite- and oxalate-extractable Fe and Al as aids in
671 differentiating various classes of soils. Canadian Journal of Soil Science 46, 13–22.
672 Mehra, O.P. and M.L. Jackson (1960) Iron oxide removal from soils and clays by a dithionite-
673 citrate system buffered with sodium bicarbonate. 7th National Conference on Clays and
674 Clay Minerals, 317–327.
675 Mikutta, C., J.G. Wiederhold, O.A. Cirpka, T.B. Hofstetter, B. Bourdon, U. von Gunten (2009)
676 Iron isotope fractionation and atom exchange during sorption of ferrous iron to mineral
677 surfaces. Geochimica et Cosmochimica Acta 73, 1795–1812.

678 Oni, O., T. Miyatake, S. Kasten, T. Richter-Heitmann, D. Fischer, L. Wagenknecht, A. Kulkarni,
679 M. Blumers, S.I. Shylin, V. Ksenofontov, B.F.O. Costa, G. Klingelhöfer, and M.W. Friedrich
680 (2015) Distinct microbial populations are tightly linked to the profile of dissolved iron in the
681 methanic sediments of the Helgoland mud area, North Sea. Frontiers in Microbiology, doi:
682 10.3389/fmicb.2015.0036.
683 Phillips, E.J.P. and D.R. Lovley (1987) Determination of Fe(III) and Fe(II) in oxalate extracts of
684 sediment. Soil Science Society of America Journal 51, 938–941.
685 Poulton, S.W. (2003) Sulfide oxidation and iron dissolution kinetics during the reaction of
686 dissolved sulfide with ferrihydrite. Chemical Geology 202, 79-94.
687 Poulton, S.W., M.D. Krom, and R. Raiswell. (2004) A revised scheme for the reactivity of iron
688 (oxyhydr)oxide mineral towards dissolved sulfide. Geochimica et Cosmochimica Acta 68,
689 3703–3715.
690 Poulton, S.W. and D.E. Canfield (2005) Development of a sequential extraction procedure for
691 iron: implications for iron partitioning in continentally derived particulates. Chemical
692 Geology 214, 209–221.
693 Poulton, S.W. and D.E. Canfield (2011) Ferruginous conditions: A dominant feature of the
694 ocean through Earth's history. Elements 7(2), 107–112.
695 Raiswell, R., D.E. Canfield, and R.A. Berner (1994) A comparison of iron extraction methods
696 for the determination of degree of pyritisation and the recognition of iron-limited pyrite
697 formation. Chemical Geology 111, 101–110.
698 Raiswell, R., H.P. Vu, L. Brinza, L.G. Benning (2010) The determination of labile Fe in
699 ferrihydrite by ascorbic acid extraction: methodology, dissolution kinetics and loss of
700 solubility with age and de-watering. Chemical Geology 278, 70-79.

701 Raiswell and Canfield (2012) The iron biogeochemical cycle past and present. Geochemical
702 Perspectives 1(1).
703 Riedinger, N., K. Pfeifer, S. Kasten, J.F.L. Garming, C. Vogt, and C. Hensen (2005) Diagenetic
704 alteration of magnetic signals by anaerobic oxidation of methane related to a change in
705 sedimentation rate. Geochimica et Cosmochimica Acta 69(16), 4117–4126.
706 Riedinger N., M.J. Formolo, T.W. Lyons, S. Henkel, A. Beck, and S. Kasten (2014) An inorganic
707 geochemical argument for coupled anaerobic oxidation of methane and iron reduction in
708 marine sediments. Geobiology 12, 172−181.
709 Schoenberg, R. and von F. Blanckenburg (2005), An assessment of the accuracy of stable Fe
710 isotope ratio measurements on samples with organic and inorganic matrices by high-
711 resolution multicollector ICP-MS. International Journal of Mass Spectrometry 242, 257–
712 272.
713 Scholz, F., S. Severmann, J. McManus, A. Noffke, U. Lomnitz, and C. Hensen (2014) On the
714 isotope composition of reactive iron in marine sediments: Redox shuttle versus early
715 diagenesis. Chemical Geology 389, 48–59.
716 Schwertmann, U. (1964) Differenzierung der Eisenoxide des Bodens durch photochemische
717 Extraktion mit saurer Ammoniumoxalat-Lösung. Zeitschrift zur Pflanzenernährung und
718 Bodenkunde, 195, 194–202.
719 Seeberg-Elverfeldt, J., M. Schlüter, T. Feseker and M. Kölling (2005), Rhizon sampling of
720 porewaters near the sediment-water interface of aquatic systems. Limnology and
721 Oceanography: Methods 3, 361–371.
722 Segarra, K.E.A., C. Comerford, J. Slaughter, and S.B. Joye (2013). Impact of electron acceptor
723 availability on the anaerobic oxidation of methane in coastal freshwater and brackish
724 wetland sediments. Geochimica et Cosmochimica Acta 115, 15–30.

725 Severmann, S., C.M. Johnson, B.L. Beard, and J. McManus (2006) The effect of early
726 diagenesis on the Fe isotope compositions of porewaters and authigenic minerals in
727 continental margin sediments. Geochimica et Cosmochimica Acta 70, 2006–2022.
728 Severmann, S., J. McManus, W.M. Berelson, and D.E. Hammond (2010) The continental shelf
729 benthic iron flux and its isotope composition. Geochimica et Cosmochimica Acta, 74, 3984–
730 4004.
731 Sivan, O., M. Adler, A. Pearson, F. Gelman, I. Bar-Or, S.G. John, and W. Eckerte (2011)
732 Geochemical evidence for iron-mediated anaerobic oxidation of methane. Limnology and
733 Oceanography, 56(4), 1536–1544.
734 Sivan, O., G. Antler, A.V. Turchyn, J.J. Marlow, and V.J. Orphan (2014) Iron oxides stimulate
735 sulfate-driven anaerobic methane oxidation in seeps. Proceedings of the National Academy
736 of Sciences of the United States of America, 1–9.
737 Slomp, C.P., J.F.P. Malschaert, L. Lohse, and W. Van Raaphorst (1997) Iron and manganese
738 cycling in different sedimentary environments on the North Sea continental margin.
739 Continental Shelf Research 17(9), 1083-1117.
740 Staubwasser, M., F. v. Blanckenburg, and R. Schoenberg (2006) Iron isotopes in the early
741 marine diagenetic iron cycle. Geology 34, 629–632.
742 Staubwasser, M., R. Schoenberg, F. von Blanckenburg, S. Krüger, and C. Pohl (2013) Isotope
743 fractionation between dissolved and suspended particulate Fe in the oxic and anoxic water
744 column of the Baltic Sea. Biogeosciences 10, 233–245.
745 Stookey, L. (1970) Ferrozine – A new spectrophotometric reagent for iron. Analytical
746 Chemistry 42(7), 779 –781.

747 Strelow, F.W.E. (1980) Improved separation of iron from copper and other elements by
748 anion-exchange chromatography on a 4% cross-linkage resin with high concentrations of
749 hydrochloric acid. Talanta 27, 727–732.
750 Stucki, J.W., B.A. Goodman, and U. Schwertmann (Eds) (1988) Iron in soils and clay minerals.
751 D. Reidel, Dordrecht, the Netherlands.
752 Tessier, A., P.G.C. Campbell, M. Bisson, (1979) Sequential extraction procedure for the
753 speciation of particulate trace metals. Analytical Chemistry 51, 844–851.
754 Wiederhold, J.G., N. Teutsch, S.M. Kraemer, A.N. Halliday, and R. Kretschmar (2007a) Iron
755 isotope fractionation during pedogenesis in redoximorphic soils. Soil Science Society of
756 America Journal 71(6), 1840–1850.
757 Wiederhold, J.G., N. Teutsch, S.M. Kraemer, A.N. Halliday, and R. Kretzschmar (2007b) Iron
758 isotope fractionation in oxic soils by mineral weathering and podsolization. Geochimica et
759 Cosmochimica Acta 71 (23), 5821–5833.
760 Wiesli, R.A., B.L. Beard, and C.M. Johnson (2004) Experimental determination of Fe isotope
761 fractionation between aqueous Fe(II), siderite and “green rust” in abiotic systems.
762 Chemical Geology 211, 343–362.
763 Williams, A.G.B. and M.M. Scherer (2004) Spectroscopic evidence for Fe(II)-Fe(III) electron
764 transfer at the iron oxide-water interface. Environmental Science and Technology 38,
765 4782–4790.
766 Wu, L., B.L. Beard, E.E. Roden, and C.M. Johnson (2011) Stable iron isotope fractionation
767 between aqueous Fe(II) and hydrous ferric oxide. Environmental Science and Technology
768 45, 1847–1852.

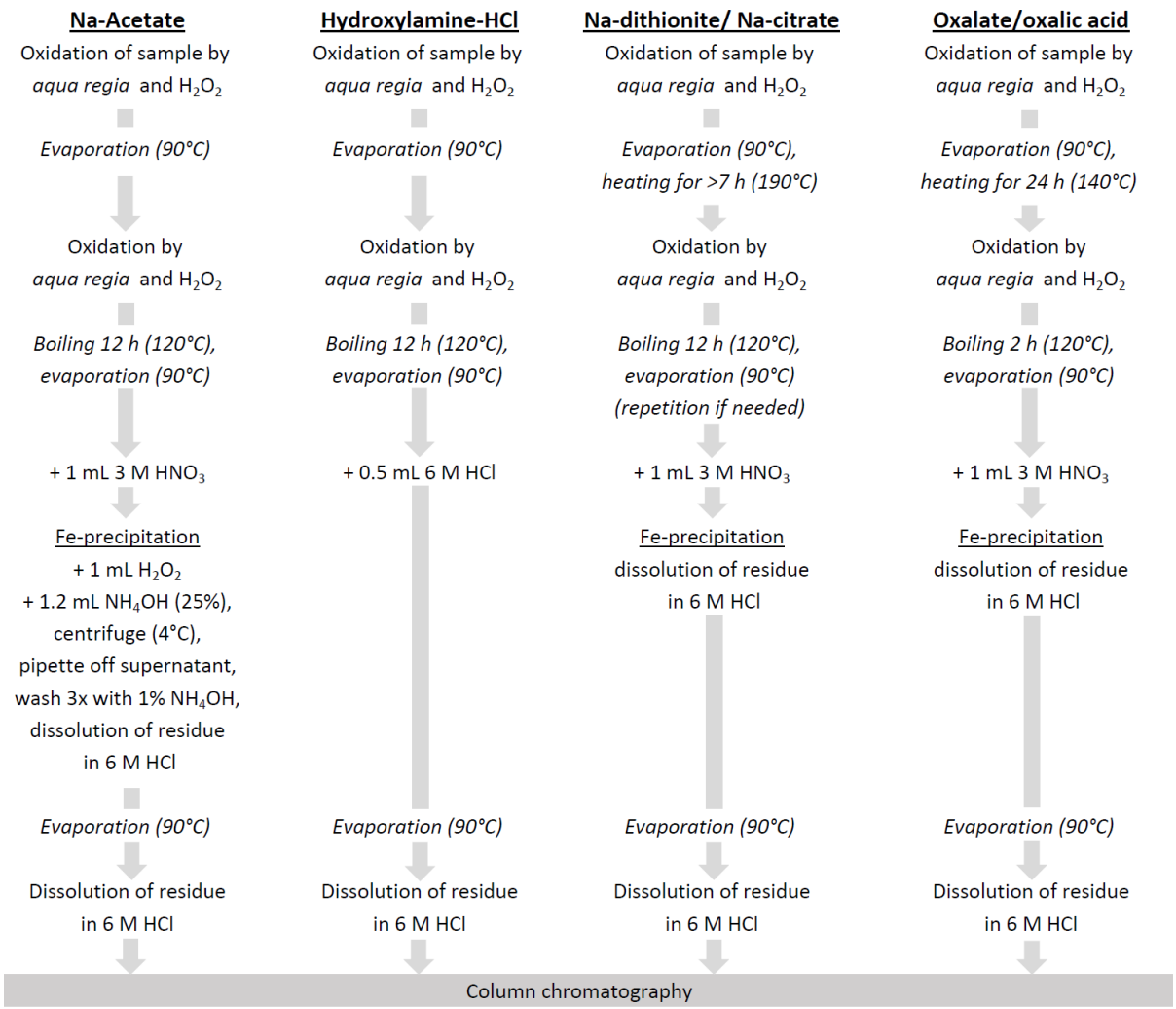

769

770 Fig. 1: Chemical processing of iron extracts for Fe isotope analysis.

771

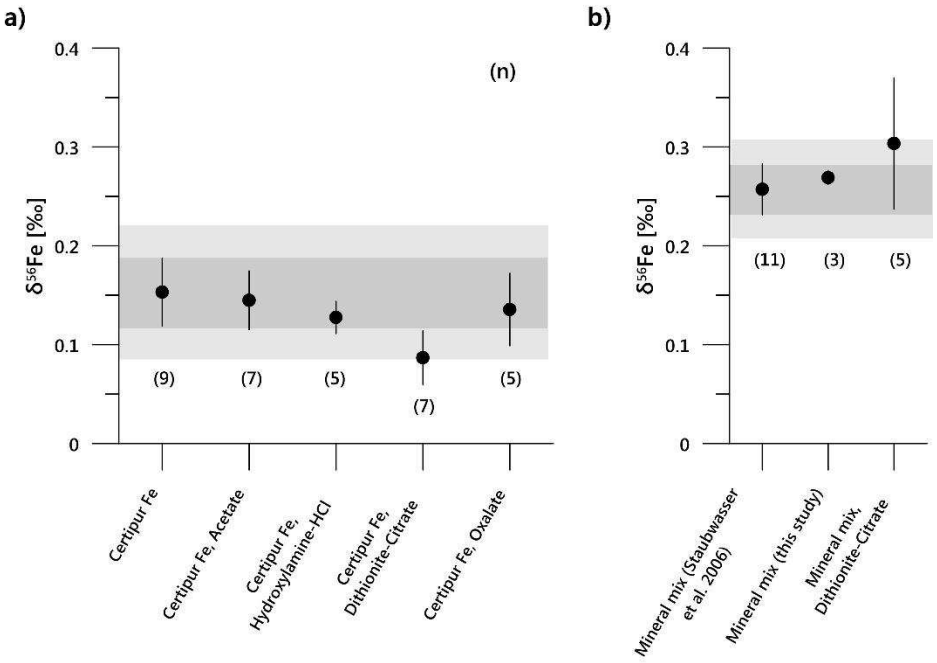

Fig. 2: Isotope data (δ^{56}Fe) of a) the Certipur® Fe solution without addition of leaching reagents and chemical processing (mineral mix, Certipur® Fe) and after addition of reagents and subsequent purification and b) of the mineral mix standard. Error bars are the standard deviation (1SD). The light greyish area indicates 2SD of the reference standard.

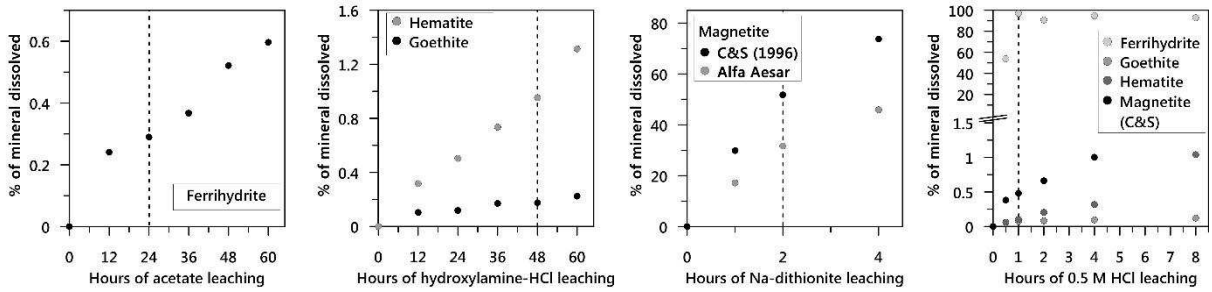

Fig. 3: Dissolution of non-target minerals by chemical treatment with acetate, hydroxylamine-HCl, Na-dithionite and dissolution of target (ferrihydrite) and non-target minerals (goethite, hematite, and magnetite) by 0.5 M HCl. The dashed lines indicate optimum extraction times for sediment samples at room temperature as given by Poulton and Canfield (2005) and Kostka and Luther (1994), respectively. Tests with dithionite were performed with magnetite synthesized after Cornell and Schwertmann (1996) and purchased from Alfa Aesar.

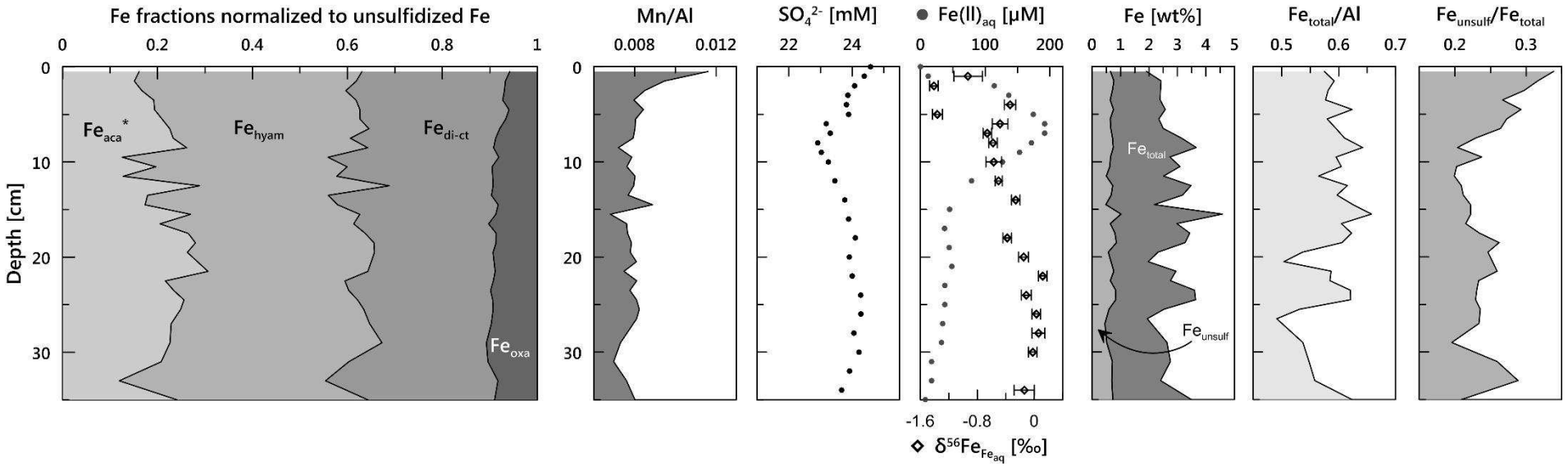

786

787 Fig. 4: Chemical data to site HE337-1 including sequentially leached Fe fractions normalized to unsulfidized reactive Fe (Fe_{unsulf} = Fe_{aca}* + Fe_{hyam} + Fe_{di-ct} + Fe_{oxa}),

788 Mn/Al, pore-water SO_4^{2-}, $Fe(II)_{aq}$, $\delta^{56}Fe_{Fe_{aq}}$, Fe_{total} and Fe_{react}, Fe_{total}/Al, and Fe_{react}/ Fe_{total}. Solid phase and pore-water data were gained for parallel cores. Fe_{aca}*

789 was corrected for Fe_{AVS}.

790

791

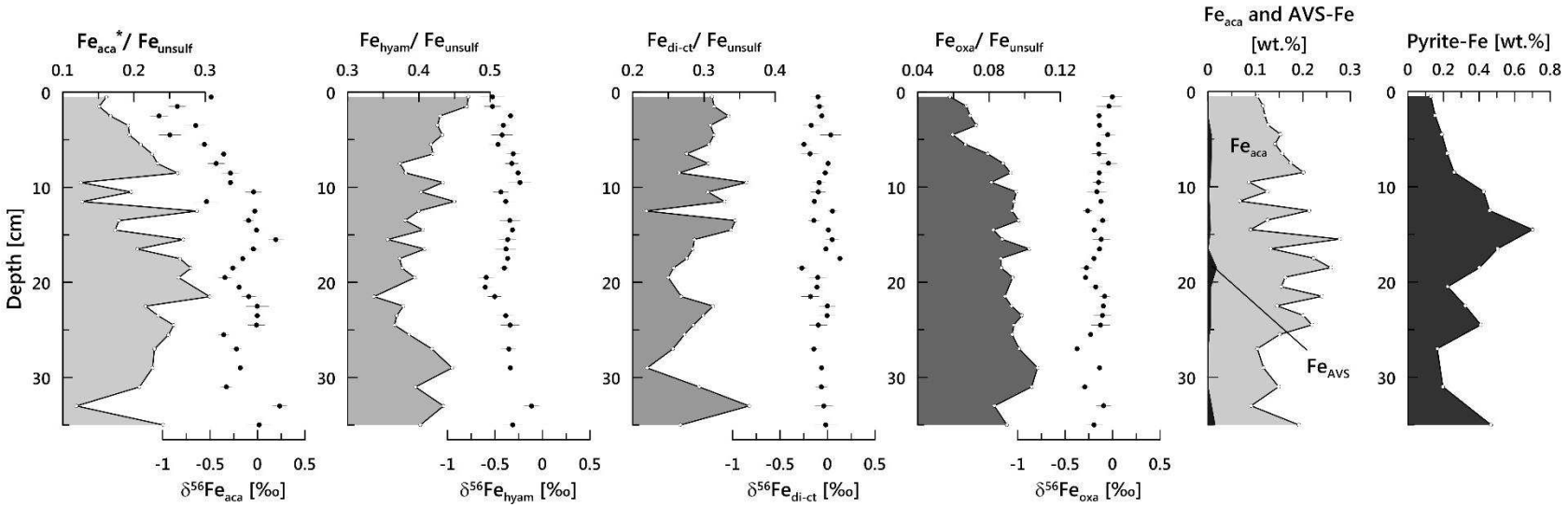

792

793 Fig. 5: Sequentially extracted Fe fractions normalized to reactive Fe and respective δ56Fe for core location HE337-1. Graphs on the left side show AVS- and

794 pyrite-Fe as determined after Canfield et al. (1986). Fe_{aca}* was corrected for Fe_{AVS}. Isotopic data is also shown in Table A.5.

795

796 Table 1: Recoveries of Certipur® Fe standard and blanks after addition and removal of extraction
797 solutions and column separation. Recoveries of Fe were normalized to standards that were
798 processed without addition of extraction reagents and chemical processing.

Extractant	Recovery of Fe (%)	n	Fe present in blanks (µg)	n
Na-Acetate	101.1 ± 1.2	6	0.2 ± 0.2	7
Hydroxylamine-HCl	101.4 ± 0.8	5	0.4 ± 0.1	9
Na-dithionite-citrate	97.5 ± 0.8	5	0.4 ± 0.4	7
Oxalate/ oxalic acid	82.9 ± 12.9	5	0.1 ± 0.1	6

799

800

801 Table 2: Selectivity of extraction steps as tested by treatment of pairs of 58Fe non-spiked and spiked
802 minerals. Isotopic ratios of mixtures and end-members are given in A.1 and A.2. C&S: magnetite
803 synthesized after Cornell and Schwertmann (1996); AA: magnetite purchased from Alfa Aesar.

Non-spiked mineral	Spiked mineral	Extractant and duration	n	Fe from mineral (in % of total dissolved Fe)		% of mineral dissolved	
				Non-spiked mineral	Spiked mineral	Non-spiked mineral	Spiked mineral
Ferrihydrite*	Goethite	Hydrox.-HCl, 48 h	3	98.5 ± 0.2	1.5 ± 0.2	87.5 ± 0.7	0.9 ± 0.3
Ferrihydrite*	Hematite	Hydrox.-HCl, 48 h	3	97.6 ± 0.6	2.4 ± 0.6	86.4 ± 1.8	1.3 ± 0.2
Goethite*	Magnetite (C&S)	Dith., 2 h	3	51.2 ± 3.5	48.8 ± 3.5	96.3 ± 3.0	74.3 ± 1.5
Hematite*	Magnetite (C&S)	Dith., 2 h	3	58.7 ± 11.0	41.3 ± 11.0	95.5 ± 9.2	63.1 ± 19.4
Magnetite (AA)	Goethite*	Dith., 2 h	2	37.4 ± 3.6	62.6 ± 3.6	33.5 ± 3.9	78.5 ± 9.6
Magnetite (AA)	Hematite*	Dith., 2 h	3	34.0 ± 3.6	67.0 ± 4.5	34.1 ± 0.9	88.0 ± 1.5
							*target mineral

804